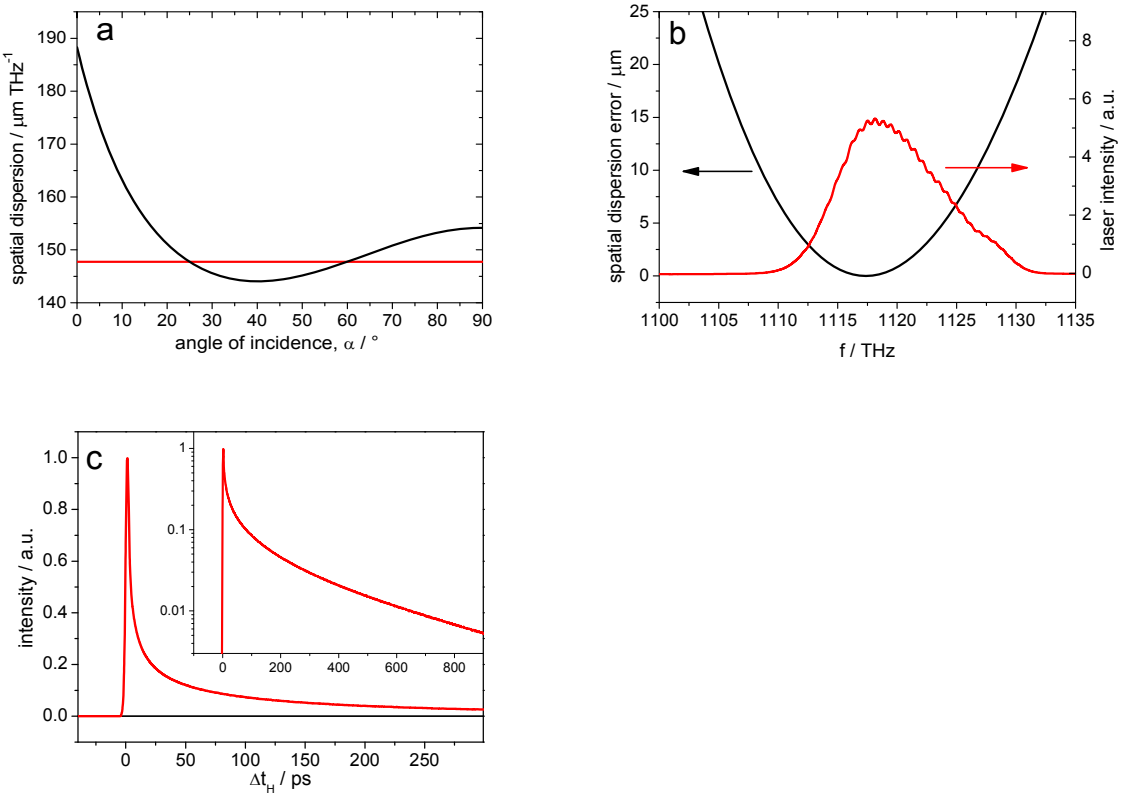

Supplementary Figure 1. Deviations of the grating spatial frequency distribution from ideality. (a) Using the parameters of Supplementary Table 1, the grating incidence angle dependence of the grating's linear spatial dispersion, Supplementary Eq. (22) (black line), is compared with the ideal linear spatial dispersion, Supplementary Eq. (21) (red line); at grating incidence angles of $\alpha = 25.0°$ and $60.0°$ they match, indicating optimal bunch-compression of the H–atom pulse at a distance of $X_0 = 44.6\ \mathrm{mm}$. (b) Spatial dispersion error introduced by the difference between the grating frequency distribution, Supplementary Eq. (19), and the ideal frequency distribution, Supplementary Eq. (15), for $\alpha = 60.0°$ (black line); the laser pulse spectrum is shown for comparison (red line). (c) Temporal shape of the H–atom pulse at the bunch-compression point calculated from the laser spectrum of (b) using Supplementary Eq. (23). The inset shows a logarithmic plot of the same data. The pulse width defined as the time window containing 50% (75%) of the H–atoms is 94 ps (300ps).

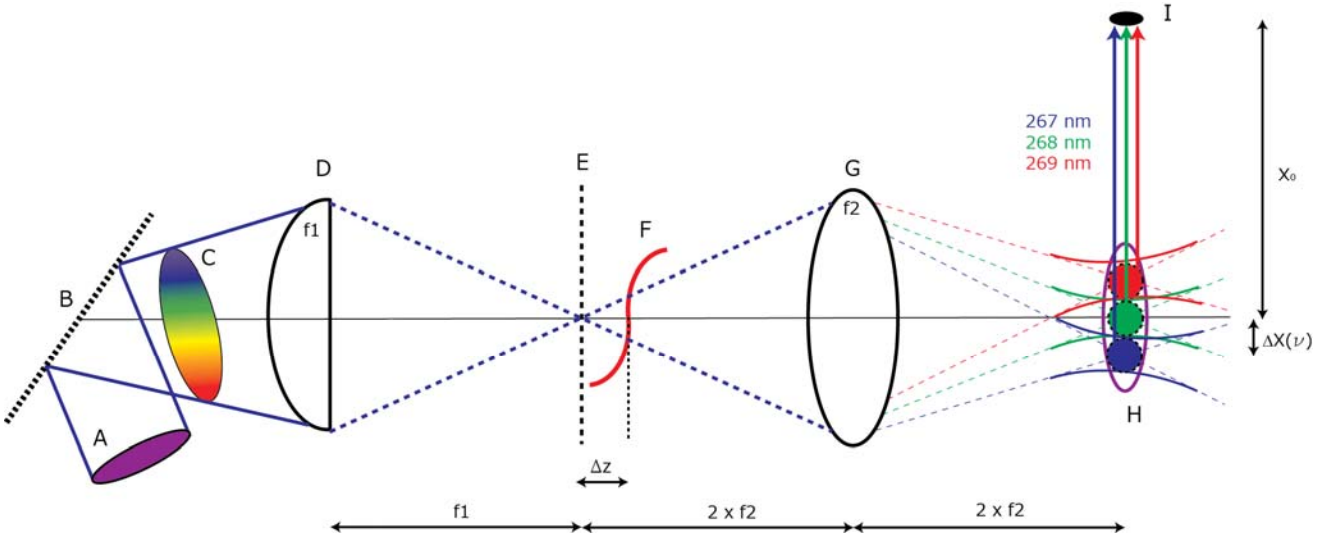

Supplementary Figure 2. Schematic setup for reducing the spatial frequency distribution error. The design of Fig. 1 is extended by an deformable mirror DM placed at a distance Δz behind the first focal plane (E). The first focal plane is imaged to the second one (H) using 1:1 optics where H–atom photoproducts are generated (for clarity the back-reflected beam propagates in forward direction at the DM).

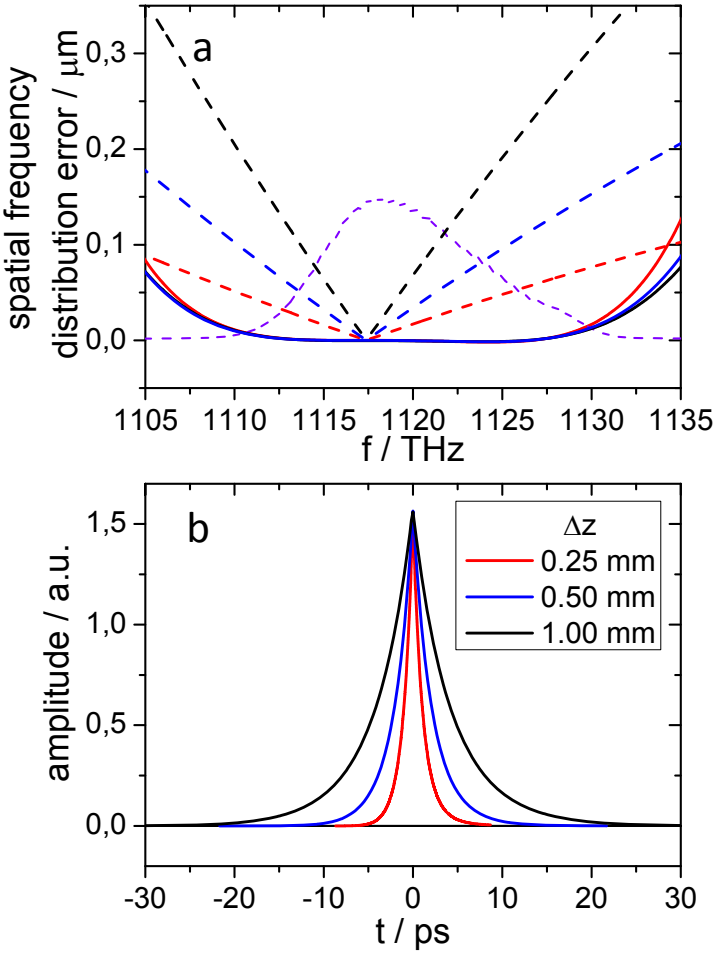

Supplementary Figure 3. Optimizing the spatial frequency distribution using a deformable mirror. (a) The spatial frequency distribution error (solid lines) is compared with the chromatic aberration error (dashed lines) for placing the DM at distances Δz = 0.25, 0.50, and 1.00 mm behind the 1st focal plane and assuming a beam diameter of 4 mm; the laser spectrum is shown for comparison (dotted line). (b) Temporal shapes of the H–atom pulse at the bunch-compression point for various Δz calculated from the laser spectrum, the chromatic aberration error and the residual spatial frequency distribution error of (a). The limits shown by these calculations are all much smaller than those due to the finite focal size of the photolysis laser, which has been neglected here.

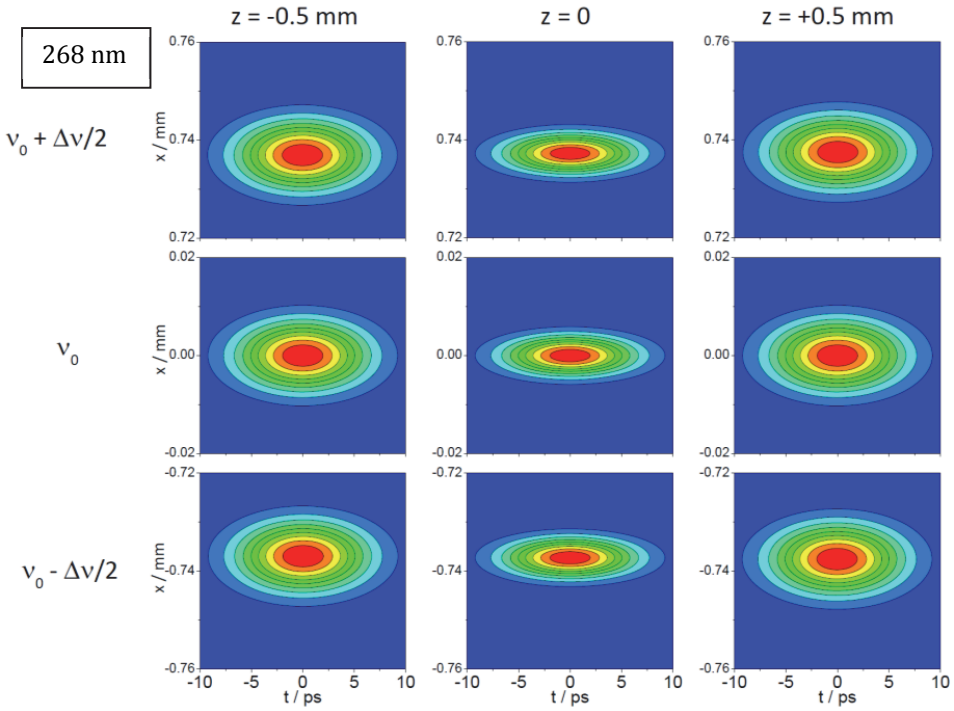

Supplementary Figure 4: Ray-pulse matrix analysis of the photodissociation pulse leading to bunch-compression. In all panels, the horizontal axis is time in ps and the vertical axis is a spatial axis, x in mm, perpendicular to the laser propagation axis, z. Moving left to right, we show calculated spatio-temporal intensity distributions for: z=–0.5 mm, z=0 and z=+0.5 mm. From top to bottom, we show three different light frequencies sampling the laser frequency bandwidth, $\Delta\nu$. One sees that in the focus (z=0) the three frequencies are spatially separated by +/– 0.74 mm and each frequency appears in a pulse of ~10 ps duration. Each frequency is focused to about 5-micron in size. At positions displaced slightly +/– 0.5 mm along z, the temporal spread is nearly unchanged and the position of the focus is altered by only about 0.4 micron – not visible to the eye. This shows that the spatial distribution of frequencies is nearly independent of z within the photolysis volume.

Supplementary Table 1. Summary of experimental conditions.

Laser pulse properties			Bunch-compression conditions	
	Pump	Probe		
ν_0 [a]	1117.4 THz	372.4 THz	X_0 [h]	44.6 mm
$\Delta\nu$ [b]	10 THz	10 THz	$v_{H,0}$ [i]	10.89 km/s
f [c]	250 mm	200 mm	k_g [j]	2400 lines/mm
w [d]	8.5±0.6 μm	125±5 μm	m [k]	1
FWHM [e]	10.2±0.7 μm	150±6 μm [f]		
z [g]	0.85 mm	1.8 mm	α [l]	60°

[a] laser center frequency
[b] laser bandwidth as a Gaussian FWHM
[c] focal length
[d] the radius at which the light intensity drops to $1/e^2$ of its maximum
[e] FWHM of the intensity profile of the laser light
[f] The effective ionization size of the probe laser is only 60 μm (FWHM) since a 6th order ionization process was used.
[g] Rayleigh length of the focus
[h] Theoretical (Experimental) bunch-compression distance for the center frequency of the photolysis laser
[i] speed of the H–atoms produced by the center frequency of the photolysis laser
[j] grating constant
[k] grating diffraction order
[l] incidence angle on the grating for optimal spatial frequency distribution

Supplementary Note 1: Conceptual treatment of Bunch-compression photolysis

Here, we explain and develop a quantitative model for the bunch-compression photolysis of HI. We begin simply with a description of the photolysis of HI using FT-limited laser pulses and assuming a point source and point detector. This is an instructive approximation to a real experiment, corresponding to the assumption that the photolysis and detection lasers are so tightly focused that we may treat them as being focused to a point. We show that as the laser pulse duration is shortened, two contributions to the H–atom pulse duration arise and show how to incorporate this in the model.

Photodissociation of HI generates hydrogen atoms with well-defined speeds. Molecular beam cooling can produce a sample of HI with essentially no internal energy. Photodissociation via the continuous A-X absorption band (280 nm > λ > 190 nm) has been thoroughly studied[1-3] and exhibits two reaction channels.

$$HI \rightarrow H + I(^2P_{3/2}) \quad \text{(A)}$$

$$HI \rightarrow H + I^*(^2P_{1/2}) \quad \text{(B)}$$

Channel (B) producing excited state I*, results in H–atoms being ejected preferentially along the laser polarization direction with a $\cos^2\theta$ angular distribution[4-6]. Channel (A) results from perpendicular transitions and leads to H–atoms with a $\sin^2\theta$ angular distribution. In these experiments we worked exclusively with channel (B); at our chosen photolysis wavelength (λ = 268.3 nm) this channel represents 45% of the photo-product flux and produces H–atoms with a nominal kinetic energy of 0.62 eV[2,3].

The speed of the H–atoms generated by channel (B) is determined by several factors involved in the conservation of energy and momentum during the photodissociation and these are represented in equations (1) and (2).

$$v_H = \sqrt{2\,E_{KIN}\frac{m_I}{m_H(m_H + m_I)}} \quad (1)$$

where E_{KIN} being the total kinetic energy release

$$E_{KIN} = h\nu + E_{HI} - D_0 - E_{I^*} \quad (2)$$

Here, hν is the photon energy, E_{HI} is HI's internal (ro-vibrational) energy prior to dissociation, D_0 (= 24632 cm^{-1}) [2] is the HI bond dissociation energy, and E_{I^*} (= 7603 cm^{-1})[7] is the electronic energy of I*($^2P_{1/2}$). For monochromatic light at λ = 268.3 nm and for the ground state of HI where $E_{HI} = 0$, the most probable H–atom velocity, $v_{H,0}$, can be easily found and is 10.89 km/s. If we now detect these H–atoms with a point detector at a distance X_0, and if we further approximate the photolysis as originating from a point, we expect a short pulse of H–atoms whose duration, Δt, is determined by the laser pulse duration, $\Delta\tau$, and a second factor, Δt_{BW}, that reflects the spread of photolysis energies in the short laser pulse.

$$\Delta t = \sqrt{\Delta\tau^2 + {\Delta t_{BW}}^2} \tag{3}$$

Here, we assume Gaussian quadrature for convolution of the two effects.

To quantify the effect of Δt_{BW}, we consider the derivative of the H–atom velocity with respect to the laser frequency.

$$\frac{dv_H(\nu)}{d\nu} = h\sqrt{\frac{m_I}{2\,m_H(m_H + m_I)(h\nu + E_{HI} - E_{I^*} - D_0)}} \tag{4}$$

In the limit of small deviations, the velocity spread resulting from the time-bandwidth limit can be approximated by equation (5).

$$\begin{aligned}\Delta v_H = \Delta\nu\,\frac{dv_H(\nu)}{d\nu} &= \Delta\nu\; h\sqrt{\frac{m_I}{2\,m_H(m_H + m_I)(h\nu + E_{HI} - E_{I^*} - D_0)}} \\ &= \Delta\nu\; h\sqrt{\frac{m_I}{2\,m_H(m_H + m_I)E_{KIN}}}\end{aligned} \tag{5}$$

From this we can obtain the contribution to the H–atom pulse duration arising from the finite bandwidth of a short FT-limited laser pulse. Again, assuming a point photolysis source, a point detector, and a flight distance, X_0, the nominal flight time is given by Eq. (6),

$$t = \frac{X_0}{v_H} \tag{6}$$

and its first derivative by Eq. (7).

$$\frac{dt}{dv_H} = \left|\frac{-X_0}{{v_H}^2}\right| = \frac{X_0}{{v_H}^2} \tag{7}$$

Hence, in a finite difference approximation, we arrive at Eq. (8).

$$\Delta t_{BW} \cong \frac{X_0}{{v_{H,0}}^2}\,\Delta v_H \tag{8}$$

Recall that $v_{H,0}$ is the nominal H–atom velocity produced by monochromatic light at the center wavelength of the laser pulse.

Inserting equation (5) into equation (8) we obtain the contribution to the atomic pulse width arising from the time-bandwidth product.

$$\Delta t_{BW} = \frac{X_0}{{v_{H,0}}^2}\, h\, \Delta\nu \sqrt{\frac{m_I}{2\, m_H (m_H + m_I)\, E_{KIN}}} \tag{9}$$

which can be simplified to Equation (10).

$$\Delta t_{BW} = \frac{X_0}{v_{H,0}}\, h\, \Delta\nu \frac{1}{2E_{KIN}} \tag{10}$$

The time-bandwidth product of FT-limited pulses with a Gaussian pulse shape, is $\Delta\nu\, \Delta\tau = 2\ln[2]/\pi$, which, within the context of Equation (10) leads to Eq. (11).

$$\Delta t_{BW} = \frac{X_0}{v_{H,0}}\, h\, \frac{\ln[2]}{\pi\, \Delta\tau} \frac{1}{E_{KIN}} \tag{11}$$

Substituting this result back into Equation (3), we find a general relation (12) for the atomic pulse duration resulting from photolysis with FT-limited laser pulses with Gaussian time profiles.

$$\Delta t = \sqrt{\Delta\tau^2 + \frac{m_H X_0^2}{2\, {E_{KIN}}^3 \Delta\tau^2} \left(\frac{h\ln[2]}{\pi}\right)^2} \tag{12}$$

Note that two physical effects represented by the two terms under the root, control the length of the atomic pulse: 1) the duration of photolysis, $\Delta\tau$, which increases with laser pulse duration and 2) the spread in photolysis energy which decreases with laser pulse duration. Therefore, a shortening of the laser pulse eventually leads to a broadening of the atomic pulse. The minimum atomic pulse duration possible, Δt_{min}, can be found from Eq. (12) and is shown in equation (13).

$$\Delta t_{min} = \sqrt{\frac{2\, \ln[2]}{\pi} h X_0 \sqrt{\frac{m_H}{2\, {E_{KIN}}^3}}} \tag{13}$$

If we insert typical numbers, e.g. X_0=10 cm, and E_{KIN}= 1 eV, we find an optimized H–atom pulse duration of 110 ps using an 80 ps laser pulse. This represents the physical limit for short pulses produced in this simple approximation, assuming an exact flight distance. This of course, neglects the finite size of the photolysis volume, which must be kept on the order of 1.2 μm (=110 ps/$v_{H,0}$) to produce such a short pulse.

We now show how the frequency spread of short FT-limited Gaussian pulses can be used to advantage, in order to increase the size of the photolysis volume by a factor of 10^3 while simultaneously producing sub-ns atomic pulses by bunch-compression.

In the following paragraphs, we present the calculations necessary for practical application of bunch-compression photolysis, assuming the photolysis and detection lasers are so tightly focused that we can ignore the finite size of the focal region. Due to the spatial distribution of frequencies used in bunch-compression photolysis, the photolysis takes place along a line in the *x*-direction of

Fig. 4. The target or detector is treated as a point. We defer the discussion of the effect of a finite photolysis and detector volumes to Supplementary Note 2.

Eq. (14) gives the flight distance, $X(\nu)$, for the photo-products generated at a given laser frequency, ν, that will be compressed at point (F) of Fig. 1.

$$X(\nu) = X_0 \frac{v_H(\nu)}{v_H(\nu_0)} \tag{14}$$

Using Eq.'s (1) and (2), we find the ideal position, X, of the focus needed for bunch-compression at a given laser frequency.

$$X(\nu) = X_0 \sqrt{\frac{h\nu + E_{HI} - D_0 - E_{I^*}}{h\nu_0 + E_{HI} - D_0 - E_{I^*}}} = X_0 \sqrt{\frac{E_{KIN}(\nu)}{E_{KIN,0}}} \tag{15}$$

where $E_{KIN,0}$ is the total kinetic energy release for HI dissociation at the central laser frequency ν_0. We refer henceforth to Eq (15) as the "*ideal spatial frequency distribution"* needed for optimal bunch-compression.

It will be convenient to define $\Delta X(\nu)$.

$$\Delta X(\nu) \equiv X(\nu) - X_0 = X_0 \left(\sqrt{\frac{E_{KIN}(\nu)}{E_{KIN,0}}} - 1 \right) \tag{16}$$

We now seek an equation analogous to Eq. (15), which describes the position of the focus of a FT-limited pulse incident upon a simple diffraction grating followed by a lens, as is used in this work. The parameters describing a diffraction grating are: the grating constant, k_g, in the dimension of lines/mm, the diffraction order m and the angle of incidence, α. For a given frequency, ν, the exit angle, β, is given by Equation (17).

$$\beta = \sin^{-1}\left(m\, k_g\, \frac{c}{\nu} - \sin\alpha \right) \tag{17}$$

Eq. (17) shows that the diffraction grating transforms a nominally parallel laser beam, which carries a frequency spread, to a divergent beam where each frequency appears at a different deflection angle, $\beta(\nu)$. We define the angular deflection, $\Delta\beta$, with respect to the deflection angle of the laser pulse's center frequency.

$$\Delta\beta(\nu) = \beta(\nu) - \beta(\nu_0) \tag{18}$$

After focusing by the lens, the spatial position of the focus, $X_g(\nu)$, is given (within the paraxial approximation) by Eq. (19). We call this henceforth the "*grating spatial frequency distribution*". Here, X_0 is defined as the focal position of ν_0.

$$X_g(\nu) = X_0 + \Delta X_g(\nu) = X_0 + \mathrm{f}\left[\sin^{-1}\left(m\, k_g\, \frac{c}{\nu_0} - \sin\alpha \right) - \sin^{-1}\left(m\, k_g\, \frac{c}{\nu} - \sin\alpha \right) \right] \tag{19}$$

By carefully choosing experimental conditions, the *grating spatial frequency distribution* can be manipulated to approximately match the *ideal spatial frequency distribution*. The goal then becomes finding the optimal experimental parameters so that Eq.'s (15) and (19) are nearly identical over the frequency range of the laser pulse. For a 100 *f*s laser pulse like the ones used in this work, the laser bandwidth is sufficiently small that the *ideal spatial frequency distribution* can be represented accurately by a first order Taylor series.

$$X(\nu) = X_0 + \frac{X_0\, h}{2E_{KIN,0}}(\nu - \nu_0) + \cdots \tag{20}$$

Then we see that the first expansion coefficient,

$$\left(\frac{dX(\nu)}{d\nu}\right)_{\nu_0} = \frac{X_0\, h}{2E_{KIN,0}} \tag{21}$$

,which we refer to as the *ideal linear spatial dispersion*, is a measure of the *ideal spatial frequency distribution* that we aim to produce with the grating/lens combination. For the conditions of our experiments (see Supplementary Table 1) this is shown as the red line in Supplementary Fig. 2a. By analogy we can represent the *grating spatial frequency distribution* as a 1st order Taylor series expansion and define the *grating linear spatial dispersion,*

$$\left(\frac{dX_g(\nu)}{d\nu}\right)_{\nu_0} = \frac{c\,\mathrm{f}\,m\,k_g}{\nu_0\sqrt{{\nu_0}^2 - \left(\nu_0 \sin\alpha - c\,m\cdot k_g\right)^2}} \tag{22}$$

One immediately sees in Supplementary Fig. 2a that the incidence angle, α, can be used to tune the *grating spatial dispersion* to match the *ideal linear spatial dispersion*. The *grating linear spatial dispersion* exactly matches the *ideal linear spatial dispersion* at two values of α. We chose $\alpha = 60.0°$ where the grating exhibited higher reflectivity. It is also advantageous to choose the incidence angle such that the *grating linear spatial dispersion* does not change rapidly with α.

The *grating spatial frequency distribution*, Eq. (19), obtained in this way necessarily deviates from the *ideal spatial frequency distribution*, Eq. (15). Supplementary Figure 2b shows the spatial frequency distribution error (solid black line) together with the spectrum of the laser pulse (solid red line) for our chosen value of α. When one weights this frequency dependent error over the spectrum of the laser pulse, the H–atom pulse shape,

$$\Delta t_H(\nu) = \frac{X_g(\nu) - X(\nu)}{v_H(\nu)} \tag{23}$$

shown in Supplementary Fig. 2c is obtained. The model shows a sharp peak with a long tail. Due to this long tail, it would be misleading to define a FWHM (<<25ps); considering for example that the time needed for 75% of the atoms to appear is ~300 ps. It is important to note that the pulse duration and pulse shape shown in Supplementary Fig. 2c is completely due to deviations between the *ideal and the actual frequency distributions*. Within the assumptions of the model presented so far,

improving the spatial frequency distributions leads to ever-shorter H–atom pulses, limited only by the pulse duration of the photolysis and detection lasers.

The *spatial frequency distribution* error can be reduced using adaptive optics. For this purpose the experimental setup of Fig. 1 is extended by a deformable mirror (DM) placed in the vicinity of the focal line (E), and a lens that images this 1st focal plane to a 2nd one where the H–atom bunch is generated with an optimized photolysis pulse as shown in Supplementary Fig. 3 (for clarity the back-reflected beam propagates in forward direction at the DM). Based on ray tracing we calculated the optimum DM shape describing its deformation as a function of the displacement from the optical axis by

$$z_{DM}(x) = ax^3 + bx^4 \qquad (24)$$

where a and b are adjustable parameters. This functional form guaranties that the center frequency is not deflected from the optical axis whereas red and blue-shifted spectral components are deflected in a manner which compensates the *spatial frequency distribution* error shown Supplementary Fig. 2b. The functionality of the DM critically depends on its displacement Δz from the 1st focal plane. If Δz is too small the curvature of the DM required to compensate the *spatial frequency distribution* error reaches the limits of current DM capability. On the other hand, chromatic aberration increases proportional to Δz and hence lengthens the H–atom pulse. Supplementary Fig. 4 shows the results of calculation for various values of Δz optimizing the mirror shape $z_{DM}(x)$. The *spatial frequency distribution* error plotted in Supplementary Fig. 4a (solid lines) is two orders of magnitude smaller than without adaptive optics (Supplementary Fig. 2b). In principle, this error can be reduced to any extent using a more flexible functional form than Eq. (24). The error due to chromatic aberration is proportional to the laser beam diameter. The dashed lines in Supplementary Fig. 4a are the results assuming a diameter of 4 mm, similar to what was used in this work. Taking these errors and the laser intensity spectrum into account, the resulting H–atom pulse shapes are presented in Supplementary Fig. 4b. Comparison with Supplementary Fig. 2c shows that with the DM the *spatial frequency distribution* error can be almost completely removed.

This means other factors limit the shortness of the H–atom pulse. In particular, the finite focusibility of light is a fundamental limit to the pulse duration in bunch-compression photolysis. In experiments similar to those presented in the main text employing, for example, 268 nm light with f/13 optics and where $v_{H,0}$=10.89 km/s, the Abbe limit forbids a focus smaller than 1.5 μm. This limits the H–atom pulse to be longer than 350 ps, assuming a molecular beam size of 0.25 mm.

Supplementary Note 2: Numerical Model

The same issues of light focusibility are true for the detection laser, since this too will introduce a spread in flight distances. In order to treat these finite size effects we constructed a numerical model simulation based on the principles above.

First, it is important to note that we employ a “short photolysis pulse approximation”. We imagine an instantaneous photolysis pulse with a position dependent frequency distribution that illuminates the HI molecular beam along the line (E) of Fig. 1. This approximation is valid since the grating/lens combination broadens the photolysis pulse to only a few ps.

In the numerical model, we define the *x*-axis as the H–atom flight direction and the *z*-axis as the propagation direction of the laser pulse(s). The origin of the coordinate system is the center of the focus formed by the center frequency, ν_0, of the photolysis laser pulse. See Fig. 4. We treat pump and probe beams as possessing Gaussian spatial intensity profiles. The focal parameters were determined experimentally, using the knife-edge method[8] and are summarized in Supplementary Table 1, together with other relevant experimental parameters.

Since the HI photolysis is a one-photon process, Eq. (25) can be used to determine the spatial profile of H–atom production within the focus of the photolysis laser pulse[9].

$$I_{PUMP}(x,y,z) = \frac{I_0}{\left[w_{PUMP}\sqrt{1+\left(\frac{z}{z_{PUMP}}\right)^2}\right]^2}\exp\left(\frac{-2\left[\left(x-\Delta X_g(\nu)\right)^2+y^2\right]}{\left[w_{PUMP}\sqrt{1+\left(\frac{z}{z_{PUMP}}\right)^2}\right]^2}\right) \qquad (25)$$

where w_{PUMP} is the focal radius , and z_{PUMP} the Rayleigh length. $\Delta X_g(\nu)$ is defined in Eq. (19) above. Note that the *x*-coordinate is associated with a specific photolysis laser frequency.

In the probe beam, the H–atoms are ionized via strong field multi-photon ionization, which we found to have a I^6 power dependence. Hence the ionization probability in the probe focus was given by Eq. (26)

$$I_{PROBE}(x,y,z) = \left[\frac{I_0}{\left[w_{PROBE}\sqrt{1+\left(\frac{z}{z_{PROBE}}\right)^2}\right]^2}\exp\left(\frac{-2\left[(x-X_0)^2+y^2\right]}{\left[w_{PROBE}\sqrt{1+\left(\frac{z}{z_{PROBE}}\right)^2}\right]^2}\right)\right]^6 \qquad (26)$$

We sequentially calculate the H–atom signal for fixed photolysis-laser frequencies. For each chosen frequency, $\Delta X_g(\nu)$ in Eq. (25) is defined. We then generate two sets of random (*x,y,z*) points. The first set extends over the volume of the photolysis laser pulse and second over the volume of the probe laser pulse. For each pair of randomly chosen points, the flight distance is defined and from the known speed (determined by ν) we compute an arrival time. The appropriate weight associated with this arrival time is given by the product of Eqs. (25) and (26), where the spatial variables are given by the coordinates of the randomly chosen point-pair. This procedure is repeated for a large number (10^6) of random point-pairs. The resulting set of amplitudes is summed in convenient time bins, e.g. 10 ps. We repeat this procedure over the frequency spectrum of the photolysis laser, weighting each binned arrival time spectrum by the intensity of the photolysis laser at that frequency. The nominal bunch-compression distance, $X_0 = 44.6$ mm, was obtained from measured absolute H–atom flight times and a knowledge of the H–atom's velocity.

This procedure is repeated for each of the rotational states of HI present in the pulsed molecular beam, since the H–atom speed depends on the HI rotational energy.

$$E_{HI}(J) = B_0\,J\,(J+1) - D\,J^2\,(J+1)^2 \qquad (27)$$

where $B_0 = 6.34196\ cm^{-1}$ is the rotational constant, $D = 2.069 \cdot 10^{-4}\ cm^{-1}$ is the centrifugal distortion constant, and J is the rotational quantum number[10].

Supplementary Note 3: Justification of the short photolysis pulse approximation

We have employed short photolysis pulse approximation in the numerical model above. Here we show in detail that this is justified. To show this explicitly, we analyze our experiment based on a fully time dependent "ray-pulse matrix" formalism[11,12]. We approximate the input photolysis laser pulse as a FT-limited Gaussian beam with a bandwidth equal to the measured bandwidth of our pulse. We then propagate the pulse with the ray pulse matrix method, across the grating and the lens and to the photolysis volume. This approach allows us to examine the temporal, spectral and spatial characteristics of the laser pulse at every position within the photolysis volume (or anywhere else along its path of propagation). Supplementary Fig. 5 shows key results of these calculations for our experiment performed at 268 nm with f/114 geometry, producing a 1.2 ns H-atom pulse.

In all panels of the figure, the horizontal axis is time in ps and the vertical axis is a spatial axis, x in mm, perpendicular to the laser propagation axis, z. As the panels move from left to right, one sees the spatio-temporal distribution of laser intensity as one moves along the laser propagation direction from 0.5 mm before focus (z=–0.5 mm), to the focus (z=0) to 0.5 mm behind the focus (z=+0.5 mm). This corresponds to the illuminated width of the molecular beam – defined by slit (E) of Fig. 4 – relevant to our experiment. In the figure from top to bottom, one sees three different light frequencies sampling the laser frequency bandwidth, $\Delta\nu$. One sees that in the focus (z=0) the three frequencies are spatially separated by $+/-$ 0.74 mm and each frequency appears in a pulse of $\sim$10 ps duration. Each frequency is focused to about 5-micron in size. At positions displaced slightly $+/-$ 0.5 mm along z, the temporal spread is nearly unchanged and the position of the focus is altered by only about 0.4 micron – not visible to the eye in Supplementary Fig. 5. This shows that the spatial distribution of frequencies is nearly independent of z within the photolysis volume.

We emphasize the key results of these fully time and space dependent calculations: 1) The light pulse as it appears in and near the focus is temporally broadened to $\sim$10 ps, 2) This temporal broadening is nearly perfectly uniform at all points within the photolysis volume, 3) the spatial distribution of frequencies is nearly independent of z.

Let us also consider the motion of HI and H in this experiment on the time scale of the temporally broadened laser pulse. The HI molecules move with a speed of 250 m/s, the H-atoms with 11,000 m/s. During the 10 ps photolysis pulse, the HI molecules move only 2.5 nanometers, while the H atoms move only 110 nanometers. For all intents and purposes, they don't move during the photolysis pulse and the idealization of an instantaneous pulse is valid.

These results demonstrate that the "short photolysis pulse approximation" is valid. A 10 ps light pulse has no measurable broadening influence on a 1.2 ns H-atom pulse. Neither is there any unexpected alteration of the spatial distribution of frequencies associated with the temporal broadening anywhere within the photolysis volume.

We have also carried out similar calculations for our proposed FEL experiment at 157 nm with f/17 optics. The results are similar. Indeed, the pulse broadening is smaller (5 ps), about half that shown in Supplementary Fig. 5. Clearly, the short photolysis pulse approximation is also valid here. That is, a 5 ps photolysis pulse cannot broaden a 110 ps H-atom pulse to any meaningful extent.

Supplementary Note 4: Physical limit to the absolute H–atom beam intensity and duration

We point out that the line-focus implementation used in this work can be modified in an important way by replacing the spherical lens shown in Fig. 1 (D) with a cylindrical lens, rotated so that its focusing action is in the plane of Fig. 1. The photolysis volume is then optimized in all three dimensions. We consider specifically the conditions for the 110 ps H–atom pulse from 157 nm HI photolysis, which could be achieved with an HGHG FEL; the photolysis volume is then 0.15 mm (x) *x* 0.5 mm (y) *x* 0.25 mm (z). The Cartesian coordinates refer to Fig. 4. When employing a strong HI molecular beam in an apparatus where photolysis is carried out 5-cm from the nozzle, the HI number density exceeds 2×10^{13} cm^{-3}. This reflects realistic molecular beam intensities for pulsed nozzles, which run close to the physical limits imposed by the formation of shock waves at the electroformed skimmers used for collimation. For HI photolysis near 157.6 nm saturation occurs near 2.5 μJ photolysis pulse energy[13], well below what can be achievable with HGHG-FEL's[14,15]. Here, the 110-ps pulse of 3.8 eV H–atoms exhibits an instantaneous beam intensity of 4×10^{16} H–atoms cm^{-2} s^{-1} 44.6 mm distant from the photolysis volume. The expected number density of the compressed pulse exceeds 1.5×10^{10} cm^{-3}.

The expected H-atom beam brightness (4×10^{16} H–atoms cm^{-2} s^{-1}) is three orders of magnitude higher than H-atom beams that are presently used in our laboratory for surface scattering experiments employing Rydberg atom tagging for detection of scattered H and D atoms. We mention this to give the reader an idea of magnitude in improvement achieved by this method over existing H atom sources.

By comparison even using a cylindrical lens, the volume necessary to limit the flight distance uncertainty in a simple focusing experiment (See Sec. S2.1) is 1.2 μm (x) x 500 μm (y) x 100 μm (z), resulting in a 100 times weaker H–atom pulse. One important but subtle aspect to the simple focusing experiment, which limits its usefulness, concerns the short Rayleigh length obtained when tightly focusing. It is for this reason that the z-dimension above cannot be larger than 100 μm, when the x-dimension is as small as 1.2 μm.

In the main article, we showed that 110 ps H-atom pulses are likely to be the shortest one could produce with this approach. This limitation is a practical one based on an optimal choice of f/number. If the f/number is too high, the focal size of individual frequency components is too large. If the f/number is too low, the Rayleigh length is too short and the usable photolysis volume becomes too small. In principle, one could produce H-atom pulses shorter than 110 ps, although their intensity may be too low to be useful.

There are fundamental limits to the H-atom pulse duration related to a temporal broadening effect induced by the grating/lens device used to produce the photolysis pulse. See Supplementary Note 3 for rigorous numerical calculations. Intuitively, one can think of our grating/lens combination as

optically similar to a monochromator. At the sample line focus, which functions as the focal exit plane of the monochromator, the grating/lens combination produces dispersion - that is, the frequency of the light depends on position along the line focus – hence a specific HI molecule does not experience the full 10 THz bandwidth of the ultrafast laser pulse. In the experiments shown in Fig. 2, this reduced bandwidth is on the order of 100 GHz. Since the time-bandwidth product – $\Delta\nu\,\Delta\tau = 2\ln[2]/\pi$ – must still hold, the effective pulse duration of the laser light is ~10 ps, substantially longer than the 150 fs input laser pulse, but still negligible compared to the H atom pulse duration. We also carried out pulse-ray matrix calculations of the pulses in this work that confirm these estimates. See Supplementary Note 3.

Under all conditions discussed in this paper, this effect is too small to be important. However, it is possible to construct experiments where the temporal broadening of the laser pulse induced by the grating is large and limiting. In particular if the bunch-compression distance, X_0, is chosen to be large and the kinetic energy of the H atom is chosen to be low. Then according to Eq. 21 the spatial dispersion becomes much larger than that used in this work. This means that each HI molecule sees an even smaller portion of the total bandwidth and the effective photolysis pulse duration is lengthened further. This points out specific conditions that should be avoided when implementing the bunch-compression photolysis technique.

Supplementary References

1 Ogilvie, J. F. Semi-experimental determination of a repulsive potential curve for hydrogen iodide. *Trans. Farad. Soc.* **67**, 2205-2215, (1971).
2 Langford, S. R., Regan, P. M., Orr-Ewing, A. J. & Ashfold, M. N. R. On the UV photodissociation dynamics of hydrogen iodide. *Chem. Phys.* **231**, 245-260, (1998).
3 Manzhos, S., Loock, H.-P., Bakker, B. L. G. & Parker, D. H. Photodissociation of hydrogen iodide in the A-band region 273--288 nm. *J. Chem. Phys.* **117**, 9347-9352, (2002).
4 Mulliken, R. S. Low Electronic States of Simple Heteropolar Diatomic Molecules: III. Hydrogen and Univalent Metal Halides. *Phys. Rev.* **51**, 310-332, (1937).
5 Clear, R. D., Riley, S. J. & Wilson, K. R. Energy partitioning and assignment of excited states in the ultraviolet photolysis of HI and DI. *J. Chem. Phys.* **63**, 1340, (1975).
6 Kitsopoulos, T. N., Buntine, A., Baldwin, D. P., Zare, R. N. & Chandler, D. W. Application of Ion Imaging to the Study of Unimolecular and Bimolecular Reactions. *SPIE* **1858**, 2-14, (1993).
7 Moore, C. E. *Atomic Energy Levels, Natl. Stand. Ref. Data Ser.*, 1971).
8 Arnaud, J. A. *et al.* Technique for Fast Measurement of Gaussian Laser Beam Parameters. *Appl. Opt.* **10**, 2775-2776, (1971).
9 The angular dependence of the photolysis probability due to the use of a polarized laser pulse is neglected.
10 Hurlock, S. C., Alexande.Rm, Rao, K. N. & Dreska, N. INFRARED BANDS OF HI AND DI. *J. Mol. Spectrosc.* **37**, 373-&, (1971).
11 Akturk, S., Gu, X., Gabolde, P. & Trebino, R. The general theory of first-order spatio-temporal distortions of Gaussian pulses and beams. *Opt. Express* **13**, 8642-8661, (2005).
12 Kostenbauder, A. G. RAY-PULSE MATRICES - A RATIONAL TREATMENT FOR DISPERSIVE OPTICAL-SYSTEMS. *IEEE Journal of Quantum Electronics* **26**, 1148-1157, (1990).
13 Brion, C. E., Dyck, M. & Cooper, G. Absolute photoabsorption cross-sections (oscillator strengths) for valence and inner shell excitations in hydrogen chloride, hydrogen bromide and hydrogen iodide. *J. Electron. Spectrosc. Relat. Phenom.* **144–147**, 127-130, (2005).
14 Yu, L. H. *et al.* High-gain harmonic-generation free-electron laser. *Science* **289**, 932-934, (2000).
15 Zhao, Z. T. *et al.* First lasing of an echo-enabled harmonic generation free-electron laser. *Nature Photonics* **6**, 360-363, (2012).